EFDA–JET–CP(08)02/15

M. Lehnen, S.S. Abdullaev, G. Arnoux, S.A. Bozhenkov, M.W. Jakubowski,
R. Jaspers, V.V. Plyusnin, V. Riccardo, U. Samma and JET EFDA contributors

Runaway Generation During Disruptions in JET and TEXTOR

Runaway Generation During Disruptions in JET and TEXTOR

M. Lehnen[1], S.S. Abdullaev[1], G. Arnoux[5], S.A. Bozhenkov[1], M.W. Jakubowski[3], R. Jaspers[2], V.V. Plyusnin[4], V. Riccardo[5], U. Samma[1]
and JET EFDA contributors*

JET-EFDA, Culham Science Centre, OX14 3DB, Abingdon, UK

[1]Institut für Plasmaphysik, Forschungszentrum Jülich, Association EURATOM-FZJ,Germany
[2]FOM-Rijnhuizen, Association EURATOM-FOM, The Netherlands
[3]Max-Planck-Institut für Plasmaphysik, IPP-EURATOM Association, Teilinstitut Greifswald, Wendelsteinstr. 1, 17491 Greifswald, Germany
[4]Association Euratom-IST, Centro de Fusao Nuclear, Lisbon, Portugal
[5]EURATOM-UKAEA Fusion Association, Culham Science Centre, OX14 3DB, Abingdon, OXON, UK
** See annex of M.L. Watkins et al, "Overview of JET Results ", (Proc. 21 st IAEA Fusion Energy Conference, Chengdu, China (2006)).*

Preprint of Paper to be submitted for publication in Proceedings of the
18th Plasma Surface Interactions in Controlled Fusion Devices, Toledo, Spain
(26th May 2008 - 30th May 2008)

ABSTRACT.
Runaway electrons generated during ITER disruptions are of concern for the itegrity of the plasma facing components. It is expected that a power of up to 8GW is exposed to ITER PFCs. We present in this article observations from JET and TEXTOR on the generation of runaways and the heat load deposition. Suppression techniques like massive gas injection and resonant magnetic perturbations are discussed.

1. INTRODUCTION

Disruptions impose severe thermal and mechanical loads on tokamak devices. This contribution focuses on Runaway Electrons (RE). During the current decay phase of a disruption, runaway electrons can be generated in present day devices with energies of some 10's of MeV. Such a runaway beam can carry up to 60% of the initial plasma current [1]. Eventually, this beam is lost to the first wall and can lead to severe damage. As this contribution will show, disruptions in today's devices do not always lead to runaway generation. The occurrence of runaways depends instead on several parameters. However, due to the strong avalanche multiplication, in ITER runaway generation is expected in every disruption [2,3]. Understanding runaway generation and developing suppression mechanisms is thus very important to avoid hazards in ITER disruptions.

In this work we present results from JET and TEXTOR disruptions. The JET results are based on a systematic analysis of 1628 disruptions. The probability for runaway generation in these disruptions depends on such parameters as the strength of the toroidal magnetic field and the electric field during the current quench. The link between high electric fields and impurity release caused by heavy wall loading during the thermal quench is demonstrated. Complementary results from TEXTOR disruptions, initiated by massive gas injection of noble gases, will also be presented. Runaway electrons can be generated deliberately by injection of about 10^{22} Argon atoms and a systematic study of their suppression by gas injection as well as their loss mechanisms has been performed. Runaway suppression can also be achieved by increasing losses using Resonant Magnetic Perturbations (RMP). The influence of n = 1 and n = 2 perturbation fields excited by the helical coils of the Dynamic Ergodic Divertor (DED) on runaway loss has been studied.

2. RUNAWAY ELECTRON GENERATION

The generation of runaways was studied, by a systematic survey of JET disruptions from pulse JPN50000 (May 2000) to JPN69626 (Januar 2007). About 8% of the pulses were terminated by a disruption. For the detection of the runaways the neutron rate is used. An increase of the neutron rate during the current quench was taken as indicator. In this way, runaway electrons with energies exceeding about 10MeV are detected. In 16% of the cases, no neutron signal was available, and these pulses are not taken into account in the analysis. Runaway electrons were detected in limiter and divertor configurations. In limiter plasmas 43% of the disruptions generate RE, in divertor configuration these are 16%. However, a large fraction of the limiter disruptions were deliberately

initiated by impurity gas puttng [4] to provoke runaway generation.

It is assumed, that significant runaway generation takes place in present day devices, when the ratio of toroidal electric field to Dreicer field is larger than 0.01 – 0.02 [5]. These runaways are the primary population, which can be multiplied by the avalanche process [6]. However, the loss by, for example, magnetic fluctuations can prevent from a significant runaway current. Because of the various factors determining the runaway generation, we have chosen in the following to present the probability for runaway generation as function of the main parameters, like e.g. electric and magnetic field.

The maximum electric field during the current quench is deduced from the maximum current decay rate $E = L_P \, dI_P/dt$, where the inductance L_P is $1{:}2\mu_0 R_0 l_i/2$ with l_i being the internal inductance as given by EFIT reconstruction before the energy quench. The inductance has been corrected by a factor resulting from the current profile flattening after the thermal quench: $3 - 2\Delta I^{max}_p / I_P$, with I^{max}_p being the maximum current of the current spike occurring after the thermal quench [7]. The probability for runaway generation is given in figure 1a as a function of the maximum electric field during the current quench. A strong increase of the RE probability is found with increasing electric field. The maximum electric field in this database is about 50V/m.

As reported earlier from JET [4,8], runaway generation occurs only above a threshold for the toroidal magnetic field of about 2T (figure 1b). This threshold is also reported from Tore Supra [9], JT-60U [10] and TEXTOR (see below) and is thus independent from machine size. Moreover, the runaway probability increases significantly for magnetic fields beyond 3T with a tendency to higher runaway currents [1].

The development of a runaway beam depends strongly on the stability of the plasma column. Plasmas which are strongly vertical unstable and soon lost to the wall do not build up a significant runaway current. This is seen from figure 1c, where the RE generation probability is plotted versus the vertical displacement at the time of the maximum electric field. The displacement is given relative to the value before the disruption. Only smaller displacements can be tolerated for runaway generation and a slightly upward moving plasma is more prone to have runaways.

The degree of conversion of thermal current to runaway current is a function of the electric field (figure 2). It increases at high electric fields up to 50% for this database. In machines like ITER, where avalanche dominates, the conversion effciency will depend only on the plasma current and not on the electric field. However, for the JET data shown here, the electric field increases with plasma current (see discussion below) and discrimination is not possible. Attempts have been made in the past to deduce the strength of the avalanche by modelling the current conversion. However, as mentioned already in [8], because of the exponential dependence of the Dreicer generation rate on parameters which are not precisely known in the current quench, like the electron density, a quantification of the avalanche in disruptions is difficult. More insight might be gained by measuring the energy spectrum of the runaways.

Figure 3 gives the parameter space in terms of toroidal magnetic and electric field for JET disruptions.

The red dots indicate disruptions with runaway generation. The electric field needed for runaway generation (green dashed curve), increases with decreasing magnetic field, or decreasing safety factor (black lines); a differentiation is not possible. The minimum magnetic field for runaway generation in TEXTOR is indicated by the blue dots in figure 3. These data points result from massive gas injection experiments using Argon (see section 5). By changing the plasma current from 250kA to 350kA, the electric field increases from 13V/m to 25V/m. In contrast to the JET observations, the threshold of $B_t \sim 2T$ is independent from E. The safety factor varies from $q_a = 5.5$ to 3.7.

3. ELECTRIC FIELD AND IMPURITY DENSITY

The electric field plays an important role as long as Dreicer generation dominates. This is evident from the exponential increase of the generation rate with E. As soon as the avalanche mechanism dominates, the total amount of runaways generated during a disruption will be almost independent from E. However, if loss mechanisms are considered to play a role, the avalanche rate, which is proportional to E, becomes important. This is especially true, if external perturbations are discussed for runaway suppression (see section 5).

The electric field is a function of the electron temperature and the plasma current according to Ohm's law: $E \sim I_P T_e^{-3/2}$. The temperature has been deduced from the current decay: $T_e = 9.2 \times 10^{-3} \mathrm{eV}. (I_P / A_P L_P \dot{I}_P)^{2/3}$, with A_P being the plasma cross-section area and the assumption $Z_{eff} = 1.0$. For the temperatures under discussion, the average charge of the carbon ions is below4. Depending on the carbon concentration, which we assume to be below 10%, the temperatures might be underestimated by up to 50%. The electric field as function of the temperature and sorted by the plasma current is given in figure 4. The temperature ranges between $T_e = 2 - 20\mathrm{eV}$.

As expected, T_e tends to increase with higher plasma currents. At constant I_P , the electric field is increasing with impurity concentration, here carbon density. The carbon density, indicated by the dotted lines, is calculated from modified corona equilibrium [11] for a constant electron density of $n_e = 4 \times 10^{19\mathrm{m}\text{-}3}$.For constant carbon density, an increase in plasma current, does not lead to an increase in E. However, a trend of increasing carbon density with plasma current can be seen. This could be attributed to an increased inward mixing of the carbon during the energy quench for high I_P and/or to an increased carbon release. Figure 5 shows that the electric field increases with peak radiated power P_{rad} and with the maximum neutral density after the disruption n_0^{max}. The impurity release depends on the energy lost during the disruption. This is indicated by an increasing carbon deposition [12] and particle release [13] at higher thermal energies.

4. RUNAWAY DYNAMICS AND WALL INTERACTION

The heat flux limit for transient heat loads can be deduced from the one dimensional solution of the heat diffusion equation in a semi-in¯nite solid [14].These limits are defined by the melting/ sublimation temperature of the PFC material and are $15\mathrm{MWm}^{-2}\mathrm{s}^{0.5}$ for beryllium and about 40 -$60\mathrm{MWm}^{-2}\mathrm{s}^{0.5}$ for graphite and tungsten. These estimates are valid, if the heat is deposited at the

surface of the PFC. However, because of the high energies in the MeV range, the runaways have a non-negligible penetration depth. Assuming an exponential radial decay of the energy deposition, an analytical formula for the temperature increase can be found [15]:

$$\Delta T = \frac{2q}{K\sqrt{\pi}}\sqrt{\kappa \Delta t} + \frac{q\delta}{K}\left(\exp\left(\delta^2 \kappa \Delta t\right)\mathrm{erfc}\left(\delta\sqrt{\kappa \Delta t}\right) - 1\right), \quad (1)$$

where $\kappa = K/pc$, K is the heat conductivity, c the heat capacity, and ρ the density. δ is the radial e-folding length of the heat source and q is the heat flux density. The deposition duration can be estimated from the final decay of the runaway current: $\tau_{loss} = I_{RE}(dI_{RE}=dt)^{-1}$. This value varies between 2ms and 5ms for JET runaway disruptions (figure 6). The penetration depth in B_e and C is 2.5mm and 2.0mm, respectively [16]. The penetration in W is 0:15mm. A mean energy of 12.5 MeV is assumed, which is expected after avalanching [6]. Runaways generated by the Dreicer mechanism gain even higher energies and would penetrate deeper. The resulting critical energy densities are: $6MJm^{-2}$ for Be, 3-$5MJm^{-2}$ for W, and 11-$13MJm^{-2}$ for C. These values are significantly larger compared to those for surface deposition: 6-8.5 times for Be, 4.5-6.5 times for C. Because of the shallow penetration, they remain almost unchanged for W. The minimum wetted area needed to prevent from melting/sublimation, $A_{critical}$, is summarised in table 1. The energies given here do not take into account conversion of magnetic energy as proposed in [2].

The heat load generated by runaways will be discussed in the following for the JET Pulse No: 68782. During this disruption a runaway current of 0.48MA was generated. A runaway plateau of about 5 ms is formed and the runaway beam is finally lost to the upper dump plate. The dynamics of the runaway beam can be detected by the radiation from K-shell vacancy production, which is recorded by the soft X-ray camera [8,17] (figure 7). The runaway beam builds up at the vertical center and moves then with a velocity of about 200m/s upwards while increasing in size. Finally, the beam touches the upper dump plate and releases its energy to the graphite tiles. With a beam radius of about 0.5m, a heat deposition time of 2.5ms is estimated. This value is in agreement with the current decay time $T_{loss} \approx 3ms$.

The impact of the runaway beam is detected by the wide angle IR camera (figure 8). Two frames have been recorded during the disruption. The first frame shows a strong temperature increase in the divertor and at the inner poloidal limiter caused by the heat flux during the energy quench. However, on the second frame recorded 20ms later, a temperature rise at the upper dump plate is visible, which can be attributed to the impact of the runaway beam.This frame is shown in figure 8a. A detail of the upper plate is seen in figure 8b, giving the temperature difference between the two frames. The maximum temperature rise is about 530K. The heat is deposited on a very small area of about $0.3m^2$. The inhomogenous load might result from small misalignments of the tiles,

which become significant at shallow angles of incidence.

The heat flux density can be estimated from the above values for runaway current, loss time and runaway energy of 12.5MeV, to be $q = 400MWm^{-2}$. The assumption for the energy is supported by the observed neutron production, which has a threshold energy of about 10MeV. However, the detailed energy spectrum is unknown. According to equation 1, this heat load leads to an temperature rise of $\Delta T \approx 330K$ (δ =2 mm), well in agreement with the measurements. For surface deposition the temperature rise would have been $\Delta T \approx 1500K$.

5. RUNAWAY SUPPRESSION

Runaway generation in ITER is dominated by avalanche multiplication. Thus, a mitigation technique has to provide a reliable suppression of this avalanche mechanism. Presently, massive gas injection is discussed as a technique to mitigate forces and heat loads and also to suppress runaway generation [18 – 25]. However, the latter aim might have severe implications which are not easily overcome. Magnetic perturbations by external coils might turn out to be an alternative scheme.

5.1 MASSIVE GAS INJECTION

Suppression of runaway generation by massive gas injection requires enormous amounts of gas to be injected into the vacuum vessel. The aim is to increase the critical field for runaway generation $E_c \approx 10^{-21} n_e^*$ to values, such that $E < E_c$ is fulfilled during the current quench. Here, the density n_e represents bound and free electrons in m^{-3}. The maximum electric field in JET and TEXTOR is about 50V/m and the same value is assumed for ITER [3]. Thus, a density of $n_e^* > 5 \times 10^{22} m^{-3}$ has to be achieved for runaway suppression. Here, it has to be kept in mind, that this electric field is a mean value. Radial peaking might make higher densities necessary.

In order to determine the dimensions of the gas injection system for ITER, knowledge about the mixing effciency is important. The mixing effciency is defined as the ratio between impurity density in the current quench plasma and the mean density of atoms injected before the energy quench (amount of atoms divided by the vessel volume). The impurity density has been determined by modelling the current quench in TEXTOR disruptions [25]. The mixing effciency is a function of the gas species (figure 9): 3-6% for pure Argon injection, 15-30% for the Argon/Deuterium mixture and above 35-70% for Helium injection. Because of this scaling with impurity mass, the injection of 10^{26} particles into the ITER vessel is required for all three gas species. This results in a neutral pressure in the vessel of 400Pa and can have serious impact on vacuum systems and machine conditions. However, it has to be clearly stated, that this amount is needed for runaway suppression. The mitigation of forces is already observed for much smaller gas amounts [4,23,24].

In present day devices, the required densities for avalanche suppression have not been reached yet. The maximum achieved electron density in TEXTOR using the fast disruption mitigation valve [26] is about $n_e^* = 8 \times 10^{20} m^{-3}$. This type of valve has been recently installed at JET and is able to inject up to 6×10^{23} particles. Assuming the same mixing effciency as in TEXTOR, this will result

in an electron density of $n_e^* \times 2 = 10^{21} m^{-3}$.

5.2 RESONANT MAGNETIC PERTURBATIONS

Magnetic perturbations cause an enhanced radial loss of RE [27] and could be exploited for runaway suppression. The possibility to suppress runaway generation by using external coils was shown at JT-60 [28]. These experiments have shown that runaways are absent for a sufficiently high perturbation field with base mode number of m/n = 3/2. The effect of Resonant Magnetic Perturbations (RMP) on runaway generation has also been studied at TEXTOR during the flat-top phase of low density discharges [29,30]. The perturbation field is produced by the Dynamic Ergodic Divertor (DED) [31]. This divertor consists of 16 helical coils at the high ¯eld side of the machine. The base mode numbers of the resulting perturbation field are m/n = 12/4; 6/2; 3/1, depending on the chosen connection of the power supplies. Application of a m/n = 6/2 perturbation field during the flat-top phase caused a significant decrease of the runaway population above a certain amplitude. This technique has now been applied also to disruptions.

Runaways are deliberately generated by fast injection of 3×10^{21} Argon atoms into an ohmic plasma, with plasma current I_P = 300 kA and toroidal magnetic field B_t = 2.25T. This technique generates reliably a runaway current of 100kA at maximum, with plateaux of up to 50ms. The DED is energised 200ms before the gas injection. The current decay rate shows no dependence on the perturbation amplitude and lies between 60 and 80MA/s. Figure 10a shows the runaway current as function of the perturbation amplitude, represented in coil current normalised to the toroidal mode number. Perturbation fields with n = 1 and n = 2 were investigated. For n = 1 the runaway current is strongly reduced to about 30% of the reference current at coil currents above 1.4kA/n. Also for n = 2 a decrease of I_{RE} can be seen, although with larger scatter. This might be related to the reduced penetration depth of the n = 2 field.

Common for both con¯gurations, n = 1 and n = 2, is the full suppression of high energetic runaways (W_{RE} > 25MeV) above the threshold 1.4kA/n. This is indicated by the measurements of the synchrotron radiation using the tangential view of a fast IR camera [32]. The maximum of the radial integral from R = 1.4m to 1.9m is shown in figure 10b. Above the threshold almost all disruptions are free of high energetic runaways. The avalanche process becomes relevant if the runaways can achieve energies above 10 – 20MeV [33]. The absence of these, shows that the avalanche is successfully suppressed by RMP, which is consistent with the reduction by a factor 3 in runaway current.

With RMP it is only possible to suppress avalanche generation of runaways. The generation rate for the Dreicer mechanism increases exponentially with electric field and can't be compensated by RMP induced losses. The enhanced diffusion of thermal particles during RMP is related to a radial field line diffusion, which is described by a field line diffusion coefficient D_{fl}. High energetic electrons, however, are displaced with respect to the magnetic field line structures. It is therefore necessary to calculate the guiding-center motion of the runaways to quantify the degree of perturbation. The

field line diffusion is then replaced by a particle trajectory diffusion D_{pt}.

The critical D_{pt} needed to compensate the generation rate can be found from $D_{\perp}\delta^2 n_{RE}/\delta r^2 = nRE=n_{RE}/\tau_{sec}$ with $D_{\perp} = cD_{pt}$. The runaway generation rate is calculated according to the standard equations, which are given for example in [5,25]. For a maximum electric field of E = 50V = m a minimum diffusion coefficient of $D_{pt} = 2 \times 10^{-6} m^2/m$ follows from the above considerations. Calculations for the n = 1 experiments using the relativistic formulation of Hamiltonian equations for the guiding center motion [34], yield values of the order $2 - 5 \times 10^{-5} m^2/m$ [35]. However, the ergodisation and the related enhanced radial loss depends also on the position of the runaway beam with respect to the perturbation coils. This could also explain the two outliers in figure 10.

SUMMARY AND CONCLUSIONS

The generation of runaways is seen in 25% of all JET disruptions. This generation is strongly linked to the toroidal electric field during the current quench. The more impurities (carbon) are released during the thermal quench, the higher the electric field. In contrast to ITER, the primary runaways at JET are generated by the Dreicer mechanism. Extrapolation to ITER would need quantification of the avalanche amplification, which is extremely difficult because of the strong variation of the Dreicer generation rate.

The influence of the toroidal field and/or the safety factor on runaway generation are not fully understood. It might be related to loss mechanisms by magnetic fluctuations, to radial peaking of the electric field, or might indicate a different RE generation process as proposed in [36,37]. We discussed here only the average electric field, however, closed flux surfaces restablish during the current quench and current peaking is observed [38]. Dependence of the peaking on toroidal magnetic field is likely and could explain the larger critical average electric field for low B_t (figure3).

Observations of the heat load during runaway disruptions are rare. For the first time, the runaway impact was measured by the wide-angle IR camera at JET. This example shows, that the heat is deposited on an area of about $0.3m^2$.This area would be already marginally at the melting limit for the ITER-like wall in JET, if runaway currents of 2MA are generated (cf. table 1). If the wetted area scales simply with the square of the major radius, a wetted area of $1.5m^2$ results for ITER. This would marginally prevent from PFC damage in case of C. For Be and W melting is expected. However, the wetted area might increase if perfect alignment and shaping of the ITER PFCs is assumed. Uncertainties exist also for the runaway energy and the angle of incidence. If for example, the energy of the runaways is 50MeV, significant melting has been reported [39].

The suppression of runaway generation by massive gas injection is challenging, because of the huge amounts of gas to be injected: of the order of 10^{26} particles for ITER, if runaways have to be completely suppressed. Runaway suppression can be established by externally applied magnetic perturbations. The generation of high energetic runaways was suppressed by applying RMP with mode number n = 1, 2 in TEXTOR.

ACKNOWLEDGEMENTS

This work, supported by the European Communities under the contract of Association between EURATOM/FZJ, was carried out within the framework of the European Fusion Development Agreement. The views and opinions expressed herein do not necessarily reflect those of the European Commission.

REFERENCES

[1]. Plyusnin V. V. *et al.,* Nucl. Fusion **46** (2006) 277.
[2]. Putvinski S. V. *et al,* Plasma Phys. Control. Fusion **39** (1997) B157B171.
[3]. Hender T. C. *et al.,* Nucl. Fusion **47** (2007) S128.
[4]. Riccardo V. *et al.,* Plasma Phys. Control. Fusion **45** (2003) A269.
[5]. Helander P, Eriksson L-G, Andersson F, Plasma Phys. Control. Fusion **44** (2002) B247.
[6]. Rosenbluth M. N., Putvinski S V, Nucl. Fusion **37** (1997), 1355.
[7]. Yoshino R. *et al,* Nucl. Fusion **33** (1993) 1599.
[8]. Gill R. D. *et al.,* Nucl. Fusion **42** (2002) 1039.
[9]. Martin G. *et al.,* 22nd Eur. Physical Society Conf. on Plasma Physics and Controlled Fusion (Bournemouth) 1995, II-041.
[10]. Yoshino R. *et al,* Nucl. Fusion **39** (1999) 151.
[11]. Post D .E, J. Nucl. Mater. 220-222 (1995) 143.
[12]. Kreter A. *et al.,* this conference.
[13]. Philipps V. *et al.,* this conference.
[14]. Herrmann A, Plasma Phys. Control. Fusion **44** (2002) 883.
[15]. Carslaw H. S. and Jaeger J C, Conduction of heat in solids, Oxford Clarendon Press (1959) ISBN 0-19-853368-3
[16]. Kanaya K. and Okayama S, J. Phys. D: Appl. Phys. 5 (1972) 43.
[17]. Gill R. D. *et al.,* Nucl. Fusion **40** (2000) 163.
[18]. Finken K-H *et al.,* Nucl. Fusion **41** (2001) 1651.
[19]. Whyte D. G. *et al.,* Phys. Rev. Lett. **89** (2002) 055001.
[20]. Martin G. *et al.,* IAEA 2004
[21]. Bakhtiari M. *et al.,* Nucl. Fusion **45** (2005) 318.
[22]. Hollmann E. M. *et al.,* Nucl. Fusion **45** (2005) 1046.
[23]. Granetz R. S. *et al.,* Nucl. Fusion **47** (2007) 1086.
[24]. Pautasso G. *et al.,* Nucl. Fusion **47** (2007) 900.
[25]. Bozhenkov S. A. *et al.,* submitted to Plasma Phys. Control. Fusion
[26]. Bozhenkov S. A. *et al.,* Rev. Sci. Instrum. **78** (2007) 033503.
[27]. Helander P, Eriksson L-G, Andersson F, Phys. Plasmas **7** (2000) 4106.
[28]. Yoshino R, Tokuda S, Nucl. Fusion **40** (2000), 1293.

[29]. Finken K. H. *et al*., Nucl. Fusion **46** (2006) S139.
[30]. Finken K. H. *et al*., Nucl. Fusion **47** (2007) 91.
[31]. Finken K. H. *et al*., The structure of magnetic field in the TEXTOR-DED, Schriften des Forschungszentrum Jüulich, Energy Technology **45**, ISSN 1433-5522 (2005)
[32]. Finken K. H. *et al*., Nucl. Fusion **30** (1990) 859.
[33]. Jayakumar R, Fleischmann H. H., Zweben S J, Phys. Lett. A **172** (1993) 447.
[34]. Wingen A, Abdullaev S. S. *et al,* Nucl. Fusion **46** (2006) 941.
[35]. Lehnen M *et al*., submitted to Phys. Rev. Lett.
[36]. Martin G, 25th EPS Conference on Plasma Phys. Prague, 29 June - 3 July, 1998 ECA 22C, P-3.006
[37]. Smith H *et al*., Phys. Plasmas **12** (2005) 122505.
[38]. Loarte A, ITPA-DSOL meeting, Avila, 2008.
[39]. Maddaluno G *et al*., J. Nucl. Mater. **313-316** (2003) 651.

	TEXTOR	JET	ITER
I_{RE}[MA]	0.2	2	9
E_{RE}[MJ]	0.1	1.5	15
$A_{critical}$[m^2][3]	0.01 (C)	0.25/0.12/0.5	2.5/5/1.4 (Be/W/C)

Table: Estimated runaway current, total kinetic energy and critical wetted area to prevent from melting/sublimation.

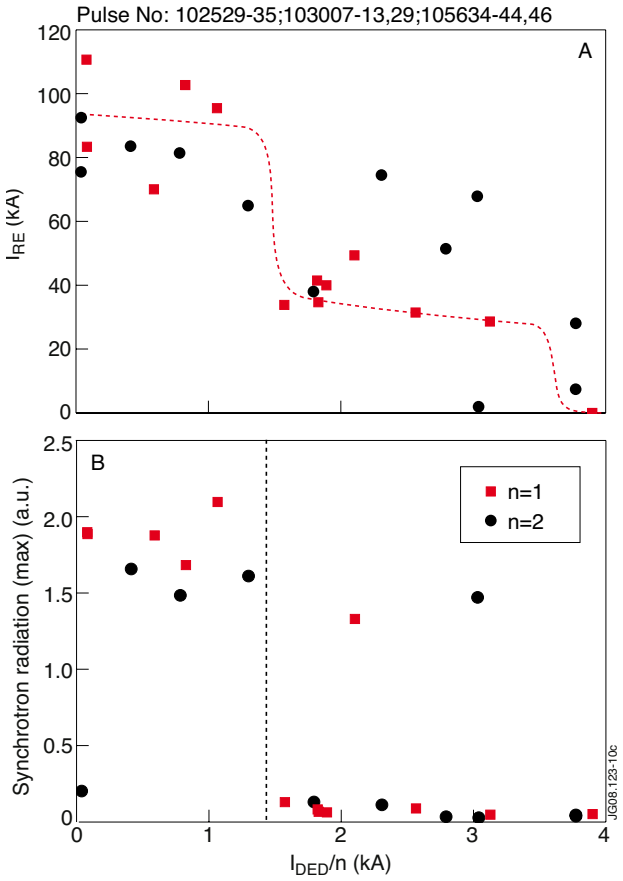

Figure 1: Probability for the generation of runaway electrons in JET disruptions (JPN50000-69626) as function of: a) the toroidal maximum electric field during the current quench, b) the toroidal magnetic field, c) the vertical displacement at the time of the maximum electric. Only divertor configurations are considered.

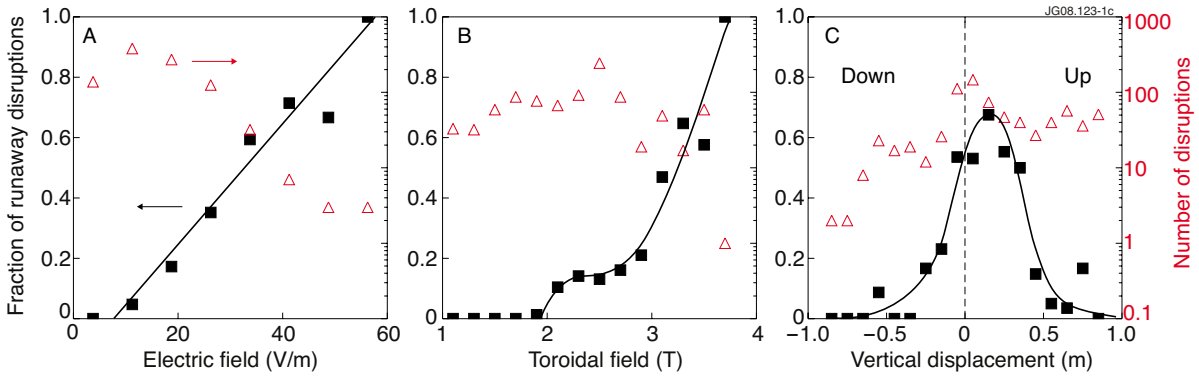

Figure 2: Runaway conversion effciency I_{RE}/I_P . The runaway current has been calculated by subtracting an exponential current decay from the measured IP. Only divertor configuration.

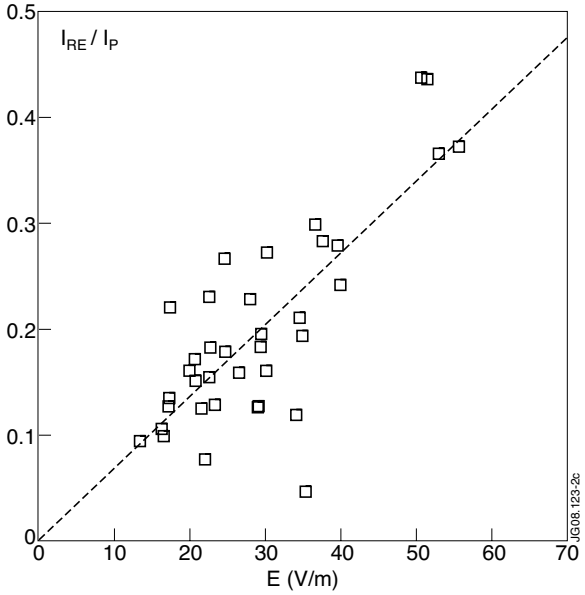

Figure 3: Parameter space for JET disruptions. The green line indicates the threshold for runaway generation. The boundary for runaway generation in TEXTOR is indicates by the blue line.

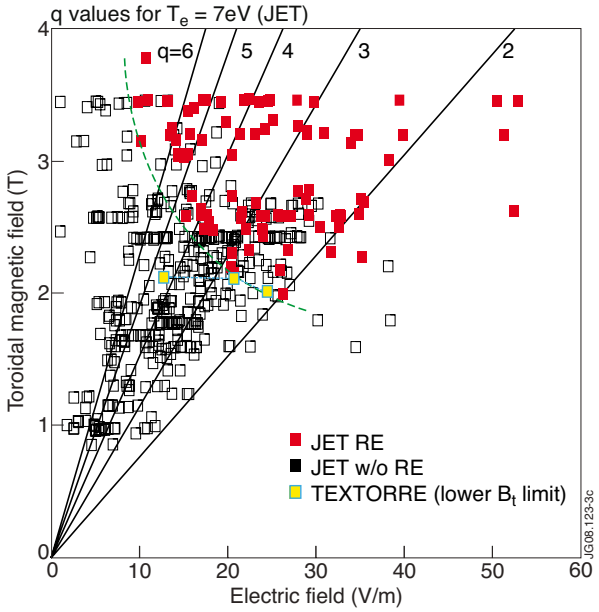

Figure 4: Toroidal electric field as function of the electron temperature T_e during the current quench. The dotted lines result from Ohm's law. The electric field deduced from the current decay is sorted by the plasma current with $\Delta I_P = \pm 0.25MA$. The electric field depends via the power balance on the carbon density: $E \sim (n_c n_e L_c(T_e))^{1/2} T_e^{-3/4}$. This dependence is indicated by the dashed brown lines for $n_e = 4 \times 10^{19} m^{-3}$.

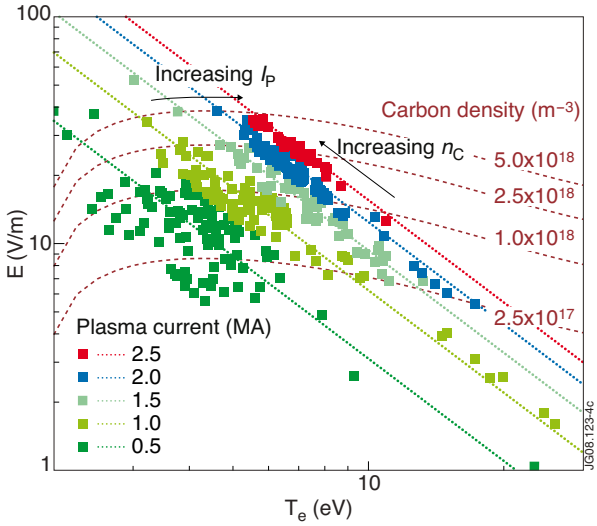

Figure 5: Electric field as function of the peak radiated power (a) and the maximum neutral density after the disruption (b). A subset of the database has been chosen for high time resolution for P_{rad} (> JPN63718). For color code see figure 4.

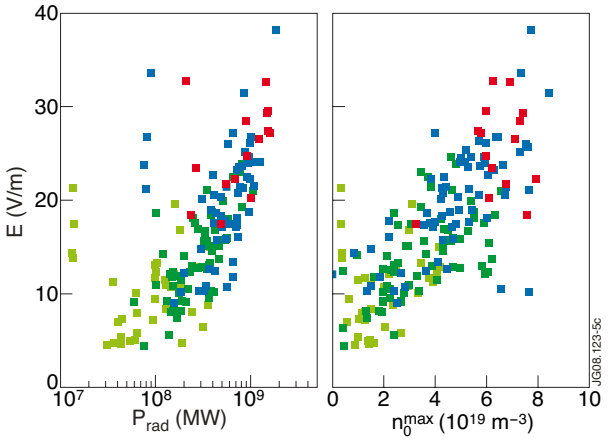

Figure 6: Decay time of the runaway current for limiter and divertor configuration.

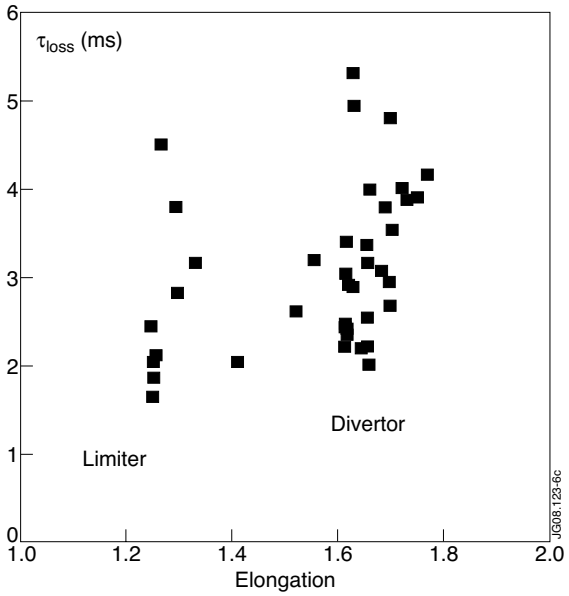

Figure 7: Soft X-ray radiation during the current quench of JET Pulse No: 68782. Because of the observation geometry, the vertical position is only indicative.

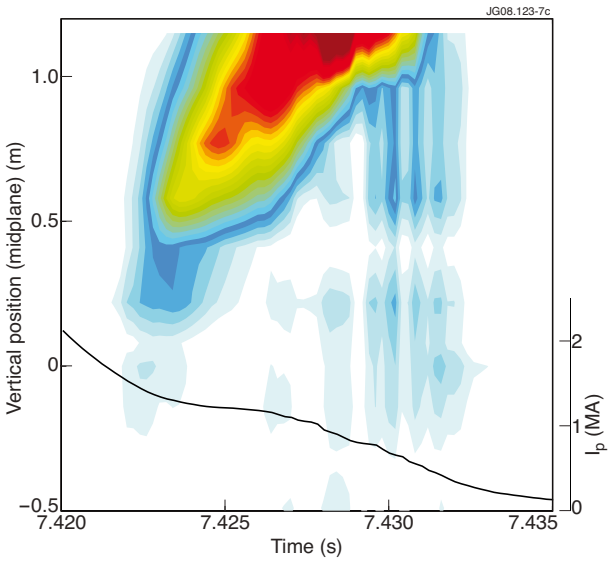

Figure 8: Heat load distribution during the disruption of JET Pulse No: 68782: a) overexposed overview frame for visualisation, b) temperature rise at the upper dump plate due to runaway impact.

Figure 9: Massive gas injection at TEXTOR: impurity mixing effciency during the thermal quench. The mixing effciency has an error of about +100%.

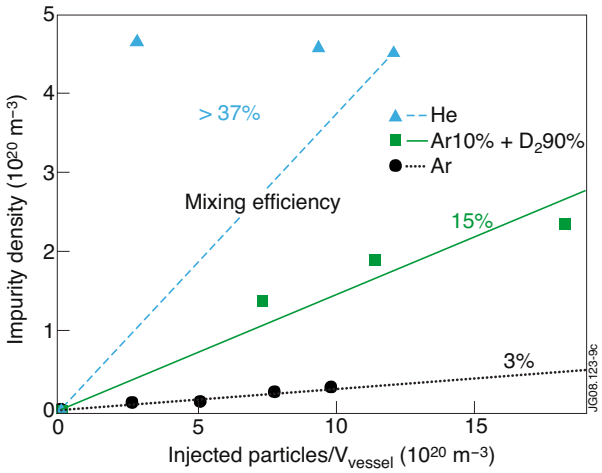

Figure 10: Runaway suppression by RMP: a) runaway current as function of the perturbation amplitude, expressed in coil current per toroidal mode number; b)maximum integral synchrotron radiation as measured by the infra-red camera.Runaways were generated by Argon injection.